Osteoblast-released Matrix Vesicles, Regulation of Activity and Composition by Sulfated and Non-sulfated Glycosaminoglycans*[S]

Johannes R. Schmidt‡§, Stefanie Kliemt‡§¶, Carolin Preissler‖, Stephanie Moeller, Martin von Bergen‡ ‡‡§§, Ute Hempel‖‖‖‖, and Stefan Kalkhof‡¶¶‖‖‖**

Our aging population has to deal with the increasing threat of age-related diseases that impair bone healing. One promising therapeutic approach involves the coating of implants with modified glycosaminoglycans (GAGs) that mimic the native bone environment and actively facilitate skeletogenesis. In previous studies, we reported that coatings containing GAGs, such as hyaluronic acid (HA) and its synthetically sulfated derivative (sHA1) as well as the naturally low-sulfated GAG chondroitin sulfate (CS1), reduce the activity of bone-resorbing osteoclasts, but they also induce functions of the bone-forming cells, the osteoblasts. However, it remained open whether GAGs influence the osteoblasts alone or whether they also directly affect the formation, composition, activity, and distribution of osteoblast-released matrix vesicles (MV), which are supposed to be the active machinery for bone formation. Here, we studied the molecular effects of sHA1, HA, and CS1 on MV activity and on the distribution of marker proteins. Furthermore, we used comparative proteomic methods to study the relative protein compositions of isolated MVs and MV-releasing osteoblasts. The MV proteome is much more strongly regulated by GAGs than the cellular proteome. GAGs, especially sHA1, were found to severely impact vesicle-extracellular matrix interaction and matrix vesicle activity, leading to stronger extracellular matrix formation and mineralization. This study shows that the regulation of MV activity is one important mode of action of GAGs and provides information on underlying molecular mechanisms. ***Molecular & Cellular Proteomics 15: 10.1074/mcp.M115.049718, 558–572, 2016.***

Skeletogenesis is a complex process that involves differentiation and proliferation, but the most important step is the mineralization of the extracellular matrix (ECM)[1] to form bone to physically support body functions (1). Our aging population is facing an increase in age-related diseases (*e.g.* diabetes and osteoporosis) that impair bone healing and require situation-adapted solutions for bone grafts and implants (2). One promising approach is the use of glycosaminoglycans (GAGs) to modify biomaterials (3). GAGs are the major organic components of ECM and play an important regulatory role in the development and remodeling of bone tissue. GAGs are polysaccharides consisting of alternating monosaccharide residues. Their sequence varies with respect to saccharide composition, glycosidic bond, and modification of the disaccharide unit, *e.g.* the degree of sulfation (3). GAGs modulate water and extracellular cation homeostasis. Moreover, they interact with and modulate the function of proteins like cytokines, adhesion molecules, and enzymes and thereby regulate processes such as migration, adhesion, differentiation, and proliferation of bone cells (2, 4–13). Thus, because human bone marrow stromal cells (hBMSC) sense their microenvironment, especially the chemical composition of the ECM (14), GAGs also promote the differentiation of bone-forming osteoblasts from hBMSC, as different studies have shown for sulfated GAGs (15, 16). Additionally, GAGs are potent molecules to promote bone anabolic activities (2).

From the ‡Department of Proteomics, Helmholtz Centre for Environmental Research UFZ, 04318 Leipzig, Germany; the ‖Institute of Physiological Chemistry, TU Dresden, 01307 Dresden, Germany; the **Biomaterials Department, INNOVENT e.V., 07745 Jena, Germany; the ‡‡Department of Metabolomics, Helmholtz Centre for Environmental Research UFZ, 04318 Leipzig, Germany; §§Department of Chemistry and Bioscience, Aalborg University, 9220 Aalborg East, Denmark; the ¶¶Department of Bioanalytics, University of Applied Sciences and Arts of Coburg, 96450 Coburg, Germany

Received March 18, 2015, and in revised form, November 2, 2015
Published, MCP Papers in Press, November 23, 2015, DOI 10.1074/mcp.M115.049718

Author contributions: M.V., U.H., and S. Kalkhof designed the research; J.R.S., S. Kliemt, C.P., and S.M. performed the research; S.M. and M.V. contributed new reagents or analytic tools; J.R.S., S. Kliemt, C.P., S.M., U.H., and S. Kalkhof analyzed the data; J.R.S., S. Kliemt, M.V., U.H., and S. Kalkhof wrote the paper.

[1] The abbreviations used are: ECM, extracellular matrix; GAG, glycosaminoglycan; hBMSC, human bone marrow stromal cell; MMP, matrix metalloproteinase; TIMP, tissue inhibitor of metalloproteinase; MV, matrix vesicle; TNAP, tissue nonspecific alkaline phosphatase; HA, hyaluronic acid; CID, collision-induced dissociation; FC, fold change; EV, extracellular vesicle; POSTN, periostin; BMP, bone morphogenetic protein; sHA1, low-sulfated hyaluronic acid.

Osteoblasts synthesize the majority of extracellular matrix components and control the mineralization of the organic ECM by secreting regulatory proteins such as osteocalcin, bone sialoprotein II, and osteoadherin and modulate the local concentration of phosphate ions by tissue nonspecific alkaline phosphatase. With ongoing differentiation, osteoblasts release matrix vesicles (MV) (17). MVs are extracellular membrane-limited structures with a diameter of 100–400 nm (18, 19). According their size and biogenesis, they are grouped into the category of ectosomes (20). Mineralizing osteoblasts as well as hypertrophic chondrocytes were shown to have high levels of Ca^{2+} ions in their mitochondria and inorganic phosphate (P_i) in their cytoplasm prior to mineralization. Ca^{2+} ions are released by mitochondria and in combination with P_i, amorphous calcium phosphate is formed at sites of MV formation (1). MVs are released from apical microvilli into the ECM by pinching off or budding (18, 19). They continue to accumulate Ca^{2+} ions and P_i, which promotes the formation of hydroxyapatite in their lumen (21). In the second phase of mineralization, MVs release hydroxyapatite crystals that propagate continuous mineral formation in the ECM (22). Furthermore, MVs possess proteins and lipids to execute essential functions for initiating mineral formation. This includes Ca^{2+}/P_i ion homeostasis, mineral nucleation, ECM remodeling, degradation of mineralization inhibitors or the maintenance of membrane lipid composition, and the control of ECM interactions that are crucial for controlling mineral growth and localization (22–24).

In previous studies we have reported that GAGs such as HA and its synthetically sulfated derivatives induce osteoblast functions, *e.g.* cell-matrix interaction, differentiation, mineralization, and endocytosis (25). However, it is not clear whether GAGs influence only the osteoblasts or also the formation, composition, activity, and adhesion to the ECM of secreted MVs. To delineate the molecular effects, the synthetically low-sulfated hyaluronic acid derivative (sHA1, degree of sulfation ~1) was studied in terms of MV biogenesis, release, and composition, and the effects were compared with those caused by naturally equally low-sulfated chondroitin sulfate (CS1, degree of sulfation ~1) as well as by non-sulfated HA. Furthermore, we isolated MVs from osteoblasts after cultivation with those GAGs and analyzed their respective protein composition in a quantitative manner using a global proteomic approach after stable isotope labeling by amino acids in cell culture (SILAC) labeling. To find out whether the alteration of the MV proteome is a reflection of the changes of the cellular proteome or whether the MV proteome is independently regulated, we compared the GAG-induced changes in both proteomes.

MATERIALS AND METHODS

Preparation of Glycosaminoglycans—Chondroitin sulfate (CS1) from porcine trachea (CS-A/C, a mixture of 70% chondroitin 4-sulfate and 30% chondroitin 6-sulfate) was purchased from Kraeber & Co. GmbH (Ellerbek, Germany). Low molecular weight HA and low-sulfated hyaluronic acid (sHA1) were synthesized and characterized as described by Kunze *et al.* and Hintze *et al.* (6, 7). Chemical properties are listed in supplemental Table 1. Stock solutions of sulfated GAG (20 mg/ml) and HA (5 mg/ml) were prepared in sterile PBS. For the experiments, the cells were incubated with 200 μg/ml sulfated GAG or HA in culture medium.

Isolation of hBMSC—Bone marrow aspirates were collected from healthy donors (Caucasian males, average age 33.0 $\pm$ 8.6 years) at the Bone Marrow Transplantation Centre of the University Hospital Dresden. hBMSC were isolated according to Oswald *et al.* (26). The study was approved by the local ethics commission (ethics vote no. EK114042009), and the donors gave their full consent. For the experiments, hBMSC preparations were chosen according to similar osteogenic differentiation potentials as estimated by alkaline phosphatase (TNAP) activity. Cells from different donors were treated as independent biological replicates.

Cell Culture and SILAC Labeling—Metabolic labeling of hBMSC proteins was conducted with SILAC protein identification and quantification media kit (DMEM flex) purchased from Invitrogen (Karlsruhe, Germany) as tested and described earlier for 34 days using either 0.1 mg of L-[(U-$^{13}C_6$]lysine and 0.1 mg of L-[(U-$^{13}C_6$,$^{15}N_4$]arginine ("heavy") or non-labeled lysine and arginine ("light") in Dulbecco's modified Eagle medium (DMEM, Biochrom KG, Berlin, Germany) (25). 7,000 hBMSC/cm were cultured onto TCPS. After 24 h, heavily labeled cells were incubated with sHA1 (reference sample), whereas lightly labeled cells were either treated with HA or CS1 (200 μg/ml each) or were not treated (control). hBMSC were grown in osteogenic differentiation medium (DMEM basal medium with 10% HI-FCS, 0.2% penicillin/streptomycin, 10 mM β-glycerophosphate, 0.3 mM ascorbic acid containing either labeled or non-labeled L-lysine and L-arginine) from day 4 on to induce osteogenic differentiation. The medium was changed every 3–4 days with osteogenic differentiation medium supplemented with GAGs as stated above.

Isolation of MVs by Ultracentrifugation—Conditioned medium containing released MVs was collected at every change of culture medium until day 22 and stored at −80 °C until MV preparation. MVs were separated by ultra-centrifugation according Xiao *et al.* (24). Briefly, conditioned medium was pre-cleared by the following centrifugation steps: 300 × *g* at 25 °C for 5 min and 20,000 × *g* at 4 °C for 30 min (2–15 and 3K30, respectively, Sigma GmbH, Osterode, Germany). For pelleting of MVs, the supernatants were subjected to an ultracentrifuge (Optima LE-80K, fixed-angle rotor 45Ti, Beckman Coulter GmbH, Krefeld, Germany) and centrifuged at 100,000 × *g* at 4 °C for 60 min. Pellets were then washed once with PBS and centrifuged again at 100,000 × *g* for 60 min at 4 °C. For nano-LC-ESI-MS/MS measurements, MV-enriched fractions were lysed in a buffer containing 6 M urea, 2 M thiourea, and 100 mM NH_4HCO_3. Protein lysate was clarified by centrifugation at 16,060 × *g* for 30 min at 4 °C (Biofuge Fresco, Heraeus, Hanau, Germany). Protein concentration of the lysate was determined by a Bradford protein assay (RotiQuant, Carl Roth GmbH, Karlsruhe, Germany) using bovine serum albumin as standard. Protein extracts were stored at −20 °C for later experiments.

Cell Harvest and ECM Preparation—At day 22 after seeding, cells were lysed in 1.5 M Tris-HCl, 1 mM $ZnCl_2$, 1 mM $MgCl_2$, and 1% Triton X-100, pH 10. To clarify the protein extracts, the samples were centrifuged at 16,060 × *g* for 30 min at 4 °C. Protein concentration of the lysate was determined by a Bradford protein assay using bovine serum albumin as standard. Protein extracts were stored at −20 °C for later experiments. For analysis of ECM-bound MVs, cells were detached from culture plates with 20 mM NH_4OH for 30 min at 25 °C. The remaining ECM was lysed in 1.5 M Tris-HCl, 1 mM $ZnCl_2$, 1 mM

$MgCl_2$, and 1% Triton X-100, pH 10, and centrifuged in the same manner as described above.

TNAP Activity—TNAP activity was determined in lysates of released matrix vesicles (100,000 × *g* fraction), cells, and ECM after detachment of cells (lysis buffer: 1.5 M Tris-HCl, 1 mM $ZnCl_2$, 1 mM $MgCl_2$, and 1% Triton X-100, pH 10) as described in Ref. 27 with *p*-nitrophenyl phosphate as a substrate. TNAP activity was calculated from a linear calibration curve ($r > 0.99$) prepared with *p*-nitrophenol. TNAP activity is given in units ($\mu mol \cdot min^{-1}$) per sample. The percentage of TNAP activity of each fraction (released MV, cells, and ECM) was calculated from the total TNAP activity of the sample.

Calcium Phosphate Accumulation—Calcium phosphate deposition by hBMSC was quantified using calcium and phosphorus kits (both from Greiner Diagnostics, Bahlingen, Germany) as described previously (28). Cell layers were washed with PBS, dried, and incubated with 0.5 M HCl at 4 °C for 24 h. Calcium and phosphate contents in the lysates were quantified photometrically with cresol phthalein complexone at 570 nm and ammonium molybdate at 340 nm, respectively. Both the calcium and phosphate contents (nmol cm^{-2}) were calculated from linear calibration curves ($p > 0.99$).

Western Blot—Western blot analysis of cell lysates was conducted as described before (29). Briefly, after SDS-PAGE (4% stacking gel, 10% resolving gel) the proteins were transferred to nitrocellulose membranes (GE Healthcare, Freiburg, Germany) by semi-dry blotting. Mouse anti-human annexin VI-IgG (clone73, BD Transduction Laboratories, Heidelberg, Germany) was applied in 25 mM Tris-buffered saline, pH 8, containing 0.5% Tween 20 and 5% bovine serum albumin overnight. Immunoreaction with horseradish peroxidase-conjugated horse anti-mouse IgG-IgG (CST, via New England Biolabs, Frankfurt/Main, Germany) was performed in 25 mM Tris-buffered saline, pH 8, containing 0.5% Tween 20 and 5% dry milk for 2 h. Visualization of the immune complex was conducted by enhanced chemiluminescence detection (GE Healthcare) using a CCD camera system (MF-ChemiBIS1.6 via Biostep Jahnsdorf, Germany). Densitometric evaluation was performed with ImageQuant 5.1 software (GE Healthcare).

Enzyme-linked Immunosorbent Assay (ELISA)—Conditioned medium of hBMSC was collected at day 22 and analyzed for the concentration of tissue inhibitor of metalloproteinase-3 (TIMP-3) using the DuoSet ELISA development kit (DY973; all from R&D systems, Wiesbaden, Germany) according to the manufacturer's instructions.

Immunofluorescence Staining—To visualize annexin V and VI at day 22, immunofluorescence staining was performed as described before (27). Briefly, after washing, fixing, and permeabilization, hBMSC were incubated with rabbit anti-human annexin V polyclonal antibody (catalog no. 8555, New England Biolabs) and mouse anti-human annexin VI monoclonal antibody (clone 73, BD Biosciences, Heidelberg, Germany) dissolved in PBS, containing 1% bovine serum albumin and 0.05% Tween 20 for 1 h. After additional washing and blocking, AlexaFluor-488-conjugated goat anti-rabbit and goat anti-mouse IgG (Invitrogen, Karlsruhe, Germany), dissolved in PBS containing 1% bovine serum albumin and 0.05% Tween 20, were used as the secondary antibody, respectively. Nuclei were stained with 0.2 μg/ml 4′,6-diamidino-2-phenylindole (DAPI), PBS for 10 min at 25 °C. Cells were embedded in Mowiol 4-88 (Sigma) and visualized using an Axiophot fluorescence microscope (Carl Zeiss, Oberkochen, Germany). The fluorescence signals were detected using the following filters: excitation 450–490 nm and emission 515–565 nm for AlexaFluor-488, and excitation 365 nm and emission 420 nm for DAPI. Digital images were obtained with an AxioCam MRm camera (Carl Zeiss) using AxioVision software release 4.6 (Carl Zeiss).

Zymography—For zymography, proteins from conditioned media were separated by one-dimensional SDS-PAGE (7.5% resolving, 4% stacking) containing 0.05% gelatin. Gels were incubated overnight in a buffer ensuring gelatinase activity (100 mM Tris-HCl, pH 7.4, 5 μM $CaCl_2$, 1 μM $ZnCl_2$). Proteins were stained with Coomassie Brilliant Blue G-250. Gelatinolytic activity associated with matrix metalloproteinase (MMP)-2 and -9 was examined by quantifying unstained bands with ImageQuant™ 5.1 software (GE Healthcare) using local median background correction.

Proteomic Sample Preparation for Nano-LC-ESI-MS/MS—Reference samples and test samples of MVs or cell extracts, respectively, were mixed and separated with SDS-PAGE on a one-dimensional gel (12% resolving and 4% stacking gel), and the resulting protein bands were stained with Coomassie Brilliant Blue G-250. The stained gel was sliced into six bands for MV samples and nine bands for cell samples with similar protein amounts, after which in-gel tryptic digestion was conducted as described before (25).

Nano-LC-ESI-MS/MS—Tryptic peptides produced by in-gel digestion from MV samples were analyzed using an LTQ Orbitrap Velos ETD mass spectrometer (Thermo Fisher Scientific, Waltham, MA) coupled with a NanoAcquity system (Waters GmbH, Eschborn, Germany). Briefly, after desalting for 8 min with 98% solvent A (0.1% formic acid in H_2O) and 2% solvent B (0.1% formic acid in H_2O) (flow rate 15 μl/min) using a 180-μm × 20-mm C18 column, tryptic peptides were applied to a 75-μm × 150-mm BEH130 C18 column (both columns by Waters). Peptide elution was achieved using a non-linear 90-min gradient of increasing solvent B (2–40%) at a flow rate of 300 nl/min. The separated peptide ions were then electrosprayed by the nano-ESI source (IonMax, Thermo Scientific, Bremen, Germany). The electrospray voltage was 1.7 kV, and normalized collision energy of 35% was used for CID-MS/MS. All MS/MS spectra were acquired in the linear ion trap by data-dependent scans in which the 10 most abundant spectra from the full MS scan (resolution of 60,000 at *m/z* 400, target value 5×10^5 counts), exceeding an intensity of 3,000, were selected for fragmentation. For CID-MS/MS, the dynamic exclusion duration was set to 120 s; the exclusion mass width was set relative to mass with 4 ppm, and the list of dynamic exclusion was limited to 500 entries.

Tryptic peptides gained from cell samples were analyzed using a LTQ Orbitrap XL ETD (Thermo Fisher Scientific) also coupled with a NanoAcquity system as described before (30). Briefly, UPLC parameters were similar to MV sample processing, but peptide elution was conducted using a non-linear 150-min gradient of increasing solvent B (1–40%). The separated peptides were electrosprayed using a chip-based electrospray device (TriVersa NanoMate ion source, Advion, Ithaca, NY) at a voltage of 1.7 kV. CID-MS/MS spectra were acquired in the ion trap by data-dependent scans in which the six most abundant spectra from the full MS scan (resolution 60,000 at *m/z* 400, target value 5×10^5 counts exceeding an intensity of 3,000) were selected for fragmentation at a normalized collision energy of 35%. The parameters for dynamic exclusion were similar to MV sample processing but the dynamic exclusion duration was set to 180 s. All MS/MS peak lists were generated using Xcalibur software (version 2.0.7 for LTQ Orbitrap XL ETD and 2.1 for LTQ Velos ETD, respectively).

Database Search—Using MaxQuant software (version 1.4.1.2) (31) with the integrated search engine Andromeda (32), the acquired MS/MS spectra were searched against a concatenated Uniprot database, which contains all reviewed human proteins (version 2nd December 2013; 39,665 sequences) as well as reverse entries and contaminants. The following MaxQuant search parameters were used: precursor's mass tolerance of 30 ppm for first search; 5 ppm for main search; fragment's ion mass tolerance 0.5 Da; two allowed missed cleavages by setting trypsin in "specific" mode as endoproteases; minimum of two peptides/protein, including at least one unique peptide. The false discovery rate for peptide and protein identification was set to 0.01 based on a target-decoy database

search. There was no threshold score set for unmodified peptides, although for modified peptides the threshold score was 40. Oxidation of methionine and acetylation of the N-terminal protein were set as variable modifications, whereas carbamidomethylation of cysteine was set as a fixed modification. Lysine 6 (^{13}C-labeled lysine) and arginine 10 (^{13}C,^{15}N-labeled arginine) were set as heavy SILAC labels. If not stated otherwise, MaxQuant default parameters were used (31). All identified contaminants from the MaxQuant integrated list were erased. Heavy/light ratios were $\log_2$-tranformed, and the median was normalized. Only proteins that were quantified in all three biological replicates were used for further analysis. The mass spectrometry proteomics data have been deposited to the ProteomeXchange Consortium (33) via the PRIDE partner repository with the dataset identifier PXD002498. Additionally, all spectra for protein annotations, based on a single unique peptide, are accessible via the web-based spectral viewer MS-Viewer (34) by the search keys oa4dn5vufr and xiztdjc0qx, respectively.

Statistical and Functional Analyses—To be considered as significantly regulated, a conservative SILAC ratio of $\log_2$ (heavy/light ratio) (fold change, FC) ≥ 0.5 or ≤ -0.5 with a p value (Student's t test, two-tail, assuming unequal variance) ≤ 0.05 needs to be fulfilled. Further biochemical data were analyzed for statistical significance with GraphPad Prism 5.04 software (Statcon, Witzenhausen, Germany) by two-way analysis of variance analysis with Bonferroni's post test. The results are presented as means ± S.E. of the mean.

For functional analysis, the list of identified proteins and their respective gene names were imported into PANTHER and clustered according their biological processes, molecular functions, cellular components, and protein classes (35). Based on those annotations and further information derived from the literature, proteins were manually classified into 11 different groups that are important for MV function and biogenesis as follows: cytoskeleton, vesicle/GTPase, metabolic process, ECM, protease and inhibitor, mineralization, cell adhesion, growth factor and receptor, protein folding, immunity and defense, and other. The isoelectric point (pI) and the molecular weight (M_r) of every protein were calculated using the ExPASy tool "Compute pI/MW." Signal peptides of all identified proteins were predicted using the SignalP 4.1 server (36). The ExoCarta database was used to evaluate the purity of the matrix vesicle proteome (37–39).

RESULTS

GAGs Affect MV Fusion and ECM Mineralization—Matrix vesicle biogenesis occurs by pinching off or polarized budding of vesicles from specific regions of the outer plasma membrane of the mineralizing cell. Annexin VI has been implicated in mediating endosome aggregation and vesicle fusion during exocytosis (1, 40). We used immunofluorescence staining and Western blot analysis to visualize the effect of the GAGs on the annexin VI level. All treatments induced an increase of annexin VI protein content (FC, 0.7–1.1) in hBMSC compared with untreated cells, but without any significant difference among the experiments (Fig. 1*A*). Immunofluorescence staining showed similar results (Fig. 1*B*); however, the distribution of annexin VI is different for sHA1. For CS1 and HA, the protein is concentrated near the nucleus and is less densely distributed over the rest of the cell in fibril structures. For sHA1, annexin VI is also mainly located near the nucleus and throughout the entire cell in dot-like structures.

Tissue-nonspecific alkaline phosphatase (TNAP), an early marker of osteogenic differentiation, hydrolyzes organic

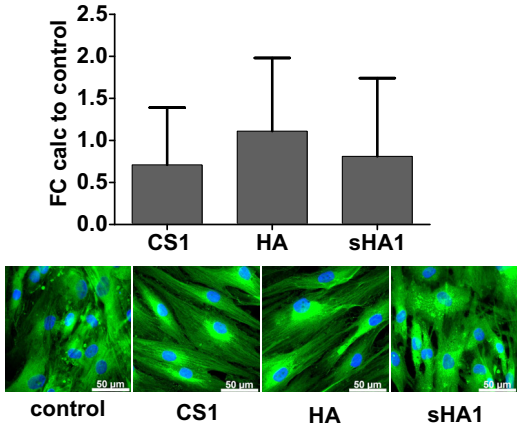

FIG. 1. **Effects of GAGs on annexin VI.** Annexin VI protein content after treatment with chondroitin sulfate (*CS1*), non-sulfated hyaluronic acid (*HA*), or low-sulfated hyaluronic acid (*sHA1*) was examined by Western blot analysis and semi-quantitative densitometric evaluation of bands, $n = 3$. Immunofluorescence images of hBMSC were stained for annexin VI (*green*) and nuclei (*blue*); *scale bar,* 50 μm.

phosphate esters such as pyrophosphate and provides inorganic phosphate to promote mineralization (41). We analyzed the influence of sHA1, HA, and CS1 on the TNAP activity of osteoblasts as well as of MVs embedded in the ECM (ECM-MV) and released MVs. HA and CS1 did not alter total TNAP activity compared with the untreated control. In contrast, sHA1 treatment resulted in a significant increase (1.7-fold, p value < 0.001; Fig. 2*A*). The relative TNAP activity per TNAP localization was not altered by the different GAGs (Fig. 2*B*).

MVs include the nucleation cores and induce formation of calcium phosphate crystals that are then released into the ECM and become part of it (1). Thereby annexin V accelerates the nucleation of an acidic phospholipid-Ca^{2+}-P_i complex on the inner MV membrane, which then triggers the *de novo* mineral formation of hydroxyapatite (1). To evaluate the calcium phosphate deposition in the hBMSC matrix, the amount of both cell-associated calcium and phosphate was quantified. As seen before for TNAP activity, sHA1 caused the greatest effects on calcium and phosphate accumulation around hBMSC. sHA1 treatment resulted in a significant increase of cell-associated calcium (2.5-fold, p value $<$ 0.01), whereas HA and CS1 showed no alteration compared with the control (Fig. 2*C*). Phosphate measurements showed the same trends, sHA1 enhanced phosphate deposition significantly (3.0-fold, $p < 0.01$) and HA or CS1 induced no changes compared with the control (Fig. 2*D*).

Immunofluorescence staining for annexin V showed a large induction of the protein in cells treated with sHA1 (Fig. 2*E*). For HA, there was no difference compared with the control, as was the case for the calcium and phosphate measurements. In contrast to those, CS1 consistently showed a slight inhibitory effect for calcium and phosphate as well as for annexin V staining. Based on these data, sHA1-treated cells were used as a reference for the quantitative proteomics study to

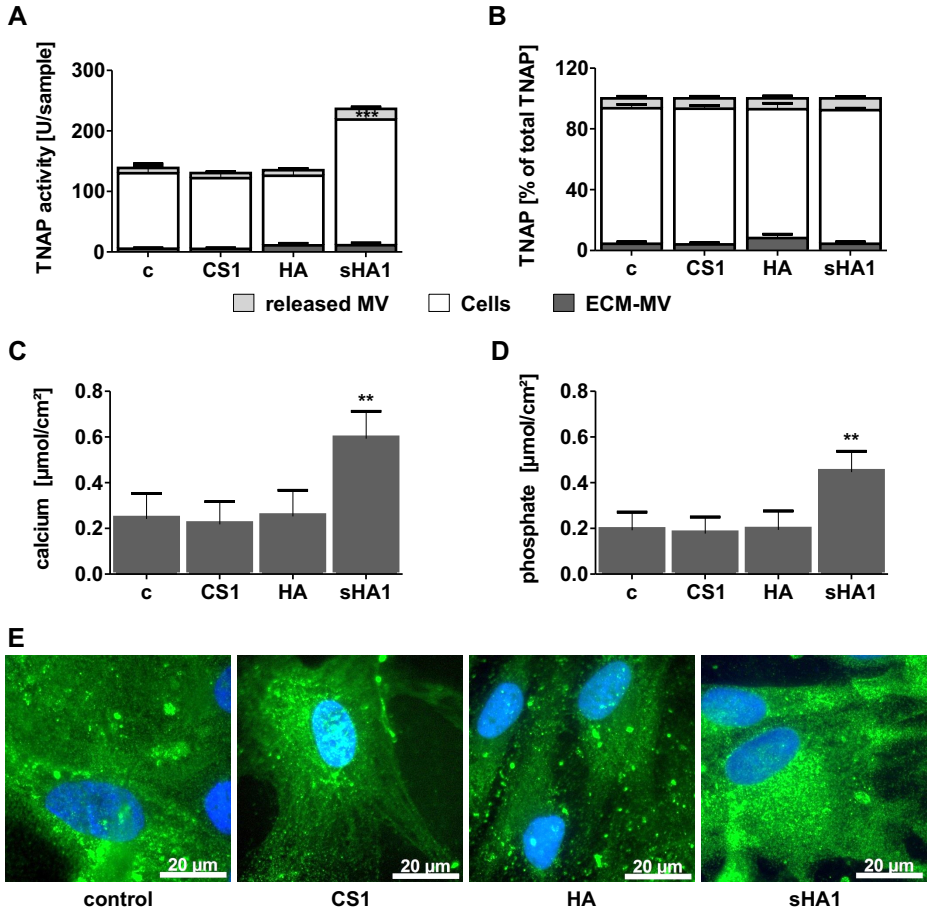

FIG. 2. **Effects of GAGs on ECM mineralization.** Degree of ECM mineralization after treatment with chondroitin sulfate (*CS1*), non-sulfated hyaluronic acid (*HA*), or low-sulfated hyaluronic acid (sHA1) is shown. TNAP activity in different fractions figured as absolute values (*A*) and proportion of total activity (*B*). The deposition of calcium (*C*) and phosphate (*D*) to the ECM is shown. Expression patterns of calcium-binding annexin V in immunofluorescence microscopy (*E*) are shown. ***, p value < 0.001; **, p value < 0.01, $n = 6$.

see whether HA and CS1 differ from sHA1 in their effect on the matrix vesicle proteome and thus on the ability of hBMSC to form bone.

Matrix Vesicle Proteome in General—SILAC-based quantitative proteomics was applied to characterize the composition of MVs released from hBMSC treated with sHA1, HA, or CS1 for 22 days. A total of 309 MV proteins with 2,218 corresponding peptides were identified (supplemental Table 2, *A* and *B*). Quantified proteins of the three treatments were normally distributed, and the correlation coefficients R^2 between the biological samples showed a linear behavior with values between 0.8 and 0.9 (supplemental Table 2*C*).

As a control for the quality of MV preparation, the presence of extracellular vesicle (EV) marker proteins, including heat shock proteins, tetraspanins, and annexins (42), was evaluated. Of the 25 most frequently identified EV proteins from the exosome database ExoCarta (37, 39, 43), 21 were found in the MV fraction (Table I). As a second criterion, all proteins identified in the MV proteome analysis were compared with all human EV proteins and all human mesenchymal stem cell (MSC) proteins available on ExoCarta. 81% of our MV dataset overlaps with the ExoCarta proteins (Fig. 3). Several studies have shown that not all EV markers are always present in all EVs (37, 39, 42, 44–47).

All 309 identified proteins were classified (Fig. 4, *A* and *B*) according to their biological processes, molecular functions, cellular components, and protein classes determined by the PANTHER classification tool (35). MVs showed no enrichment in plasma membrane proteins (3.4%), in agreement with the opinion that these vesicles do not originate to a large extent from the plasma membrane (48). Intracellular proteins (70.2%) were annotated to the cytosol and several organelles such as nucleus, ribosomes, and mitochondria. This is in line with previous findings that extravesicular proteins are associated with a variety of organelles (38). Interestingly, a high number of proteins (15%) were annotated to the category of cytoskeleton. Furthermore, 26.4% of all identified MV proteins could be classified as extracellular proteins, although this was the case for only 8.3% of the cellular proteome (supplemental Table 3*E*).

Functional clustering showed enrichment in processes that are crucial for the function of matrix vesicles and bone mineralization (Fig. 4*B* and supplemental Table 2*F*). A large number of identified proteins (15%) are involved in matrix vesicle formation and budding, such as the Rab GTPases (49). Proteins that were grouped into the cluster ECM (13%) include ECM structural proteins such as collagens or extracellular linker proteins like laminins (50). Furthermore, proteases and

TABLE I
Identification rate of 25 most prominent extracellular vesicle proteins

The 25 most frequently identified extracellular vesicle proteins from the exosome database ExoCarta were checked for identification in the matrix vesicle fraction.

Rank	Protein family	Gene name	Identified
1	Heat shock proteins	*HSPA8*	+
9		*HSP90AA1*	+
20		*HSP90AB1*	−
2	Tetraspanins	*CD9*	−
5		*CD63*	−
6		*CD81*	+
3	Metabolic enzymes	*GAPDH*	+
8		*ENO1*	+
21		*ALDOA*	+
19		*LDHA*	+
24		*PGK1*	+
11		*PKM2*	+
7	Annexins	*ANXA2*	+
23		*ANXA5*	+
4	Cytoskeletal and associated proteins	*ACTB*	+
18		*ACTG1*	+
25		*CFL1*	+
22		*MSN*	+
10	Elongation factors	*EEF1A1*	+
17		*EEF2*	−
12	14-3-3 family proteins	*YWHAE*	+
16		*YWHAZ*	+
13	Other	*SDCBP*	+
14		*PDCD6IP*	+
15		*ALB*	+

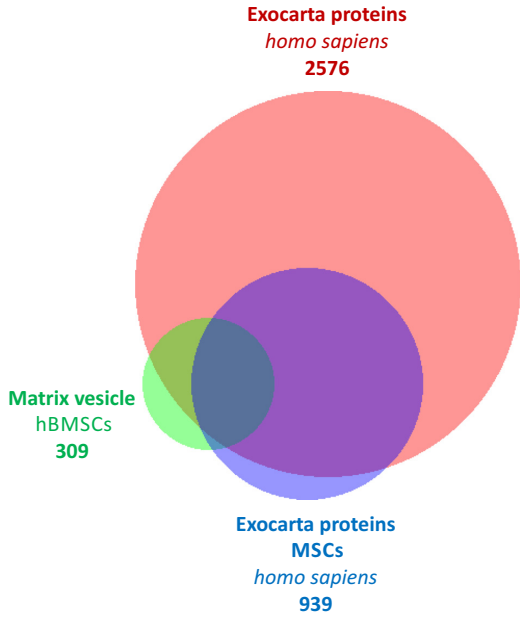

FIG. 3. **Overlap of previously reported extracellular vesicle proteins with proteins being identified in the matrix vesicle fraction.** Venn diagram showing the overlap of proteins identified in the matrix vesicle fraction (*green*) with ExoCarta database entries filtered by "human" (*red*) as well as ExoCarta database entries filtered by human and MSCs (*blue*).

their inhibitors, especially MMPs and TIMPs (51), are essential for the remodeling of the ECM and were also found to a greater extent (13%). Additionally, we identified several proteins involved in the mineralization process (9%), in particular proteins with the ability to bind calcium (annexins) and pyrophosphatase activity (guanine nucleotide-binding proteins) (52).

Besides the functional clustering, the proteomics data were analyzed concerning aspects like distribution of protein properties, *e.g.* isoelectric point (pI) and molecular weight. In regard to both parameters, the distributions of all proteins identified in the MV as well as in the cellular fraction do not significantly differ from the distribution of the human MSC dataset from ExoCarta (supplemental Table 2*D*). Furthermore, the existence of signal peptides was tested for all proteins identified in the MV fraction showing that 213 (68%) do not contain a signal peptide (supplemental Table 2*D*). This is in line with the idea that MV proteins are not released by the classical secretory pathway (48).

Influence of Various GAGs on the Matrix Vesicle Proteome

Quantified and Regulated Proteins—To investigate effects of different GAG derivatives on the MV proteome, we directly compared MV protein lysates of sHA1-treated cells to those exposed to HA, CS1, or untreated controls in a duplex SILAC approach (supplemental Table 2*E*). In each case, more than 150 proteins were quantified. Among those, the proportion of regulated proteins (fold change $> \pm 0.5$, p value < 0.05) varies between 8 and 13%.

To specify, of all 51 reliably quantified proteins (three of three replicates, ≥2 peptides) in sHA1-treated cells compared with the control, 13 were found to be up-regulated (25%), and six were down-regulated (12%). Compared with CS1-treated cells, the number of regulated proteins is similar (11 up, 18%; 10 down, 17%), whereas compared with HA the number of differentially expressed proteins is lower (10 up, 17%; 6 down, 10%), possibly indicating a higher similarity in sHA1 and HA influence on the MV proteome compared with CS1 (Fig. 5). This high proportion of regulated proteins among all reliably quantified proteins demonstrates a high impact of GAGs on MV composition.

sHA1 Affects Growth Factor Bioavailability and ECM Organization—Based on GO molecular function, GO biological process, GO cellular component, and PANTHER protein class, all proteins that were quantified in all three replicates after sHA1 treatment were manually clustered into functional groups (Fig. 6*A* and supplemental Table 2*F*).

Eight regulated proteins correspond to functional clusters that are crucial for ECM formation and mineralization. With 12 annotated proteins, the most prominent cluster constitutes the ECM-associated proteins, including three up-regulated but no down-regulated proteins. In the presence of sHA1,

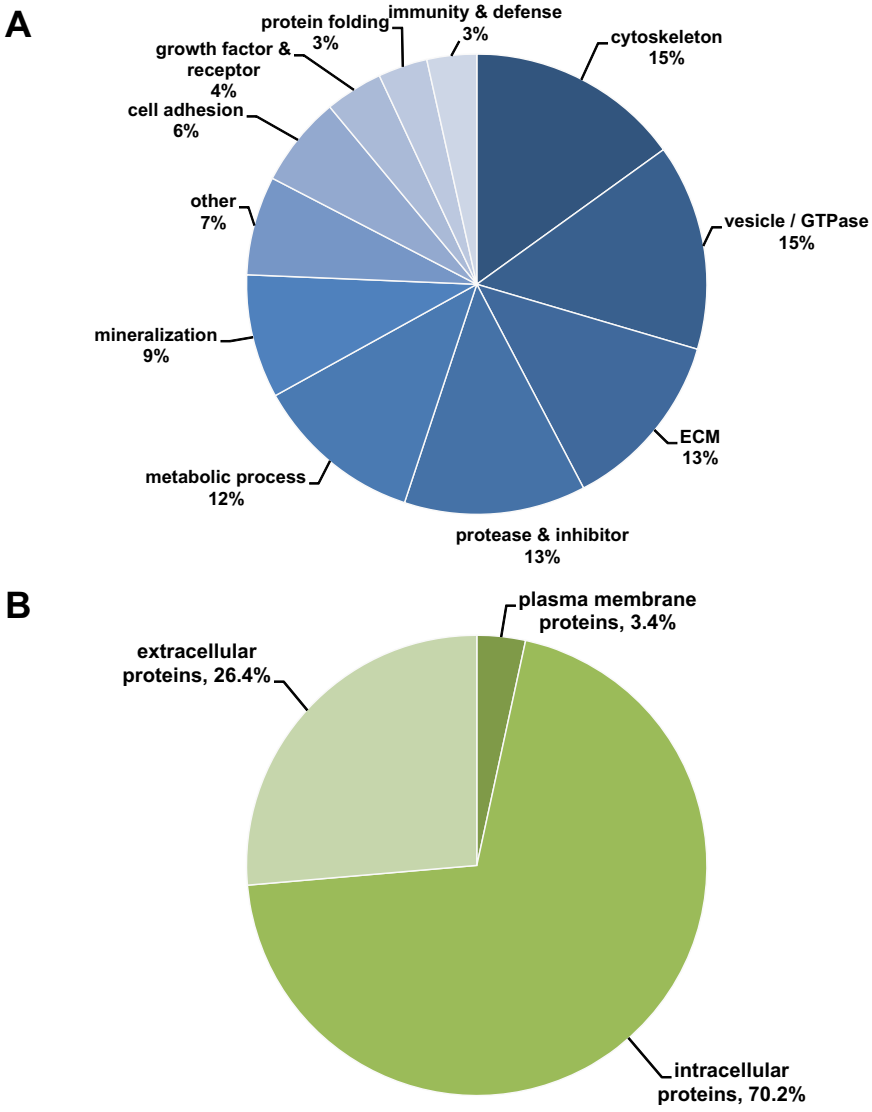

FIG. 4. **Clustering of proteins identified in the matrix vesicle fraction.** All proteins identified in the matrix vesicle fraction were clustered according to their cellular compartment (*A*) and function (*B*) using gene ontology term assignments.

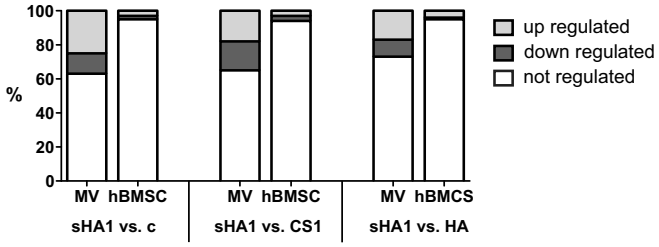

FIG. 5. **Percentage of regulated proteins after GAG treatment.** Proportion of regulated proteins among all quantified proteins in matrix vesicle and cell (hBMSC) in direct comparison of low-sulfated hyaluronic acid (*sHA1*) treatment to chondroitin sulfate (*CS1*), non-sulfated hyaluronic acid (*HA*), or no GAG treatment (*c*).

thrombospondin-1 and -2 (THBS1 and -2) are up-regulated (FC = 1.0 and 2.6). Thrombospondins are known heparin-binding proteins and seem to act as a linker between cellular membrane proteins and extracellular proteins, including transforming growth factor β family members (TGF-β) (53, 54). Additionally, both thrombospondins were shown to inhibit the catalytic activity of 72-kDa type IV collagenase (also known as matrix metalloproteinase 2, MMP2) (55). Furthermore, fibrillin-1 (FBN1) was found in higher abundance in MV after sHA1 treatment (FC = 2.7). This protein is a structural component of calcium binding extracellular 10–12-nm microfibrils that are known to regulate the osteoblast maturing by controlling TGF-β bioavailability and calibrating the local levels of TGF-β and bone morphogenetic proteins (BMPs) (56).

With four identified proteins, the functional cluster of cell adhesion is not as prominent as the ECM-associated proteins, but also among those proteins three were up-regulated. Another TGF-β-binding protein, the latent transforming growth factor β-binding protein 2 (LTBP2), was identified in higher abundance (FC = 2.5) (57). Additionally, the up-regulated fibronectin-1 (FN1, FC = 0.9) forms fibers between collagen fibrils and supports the cell adhesion by binding to

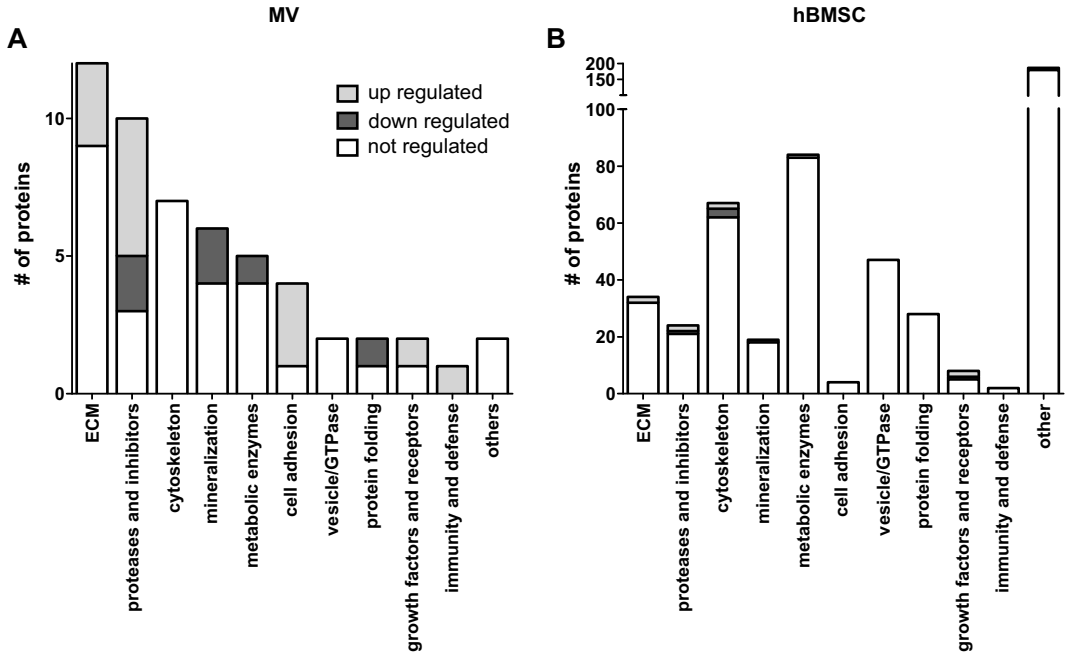

FIG. 6. **Effects of sHA1 on functional protein clusters in matrix vesicles and cellular proteome.** Number of regulated proteins among all quantified proteins with respect to functional protein clusters in matrix vesicles (*A*) and cells (*B*, hBMSC) after treatment with sHA1.

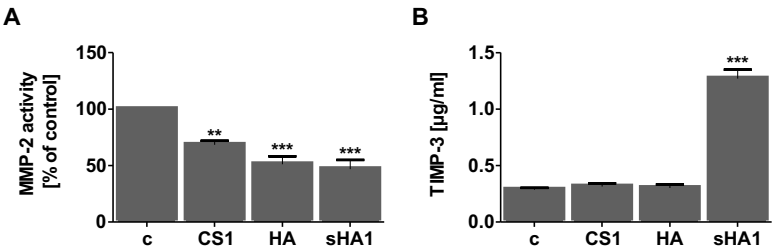

FIG. 7. **Effects of GAGs on ECM remodeling.** MMP-2 activity, as a marker for the degree of ECM remodeling, was determined after treatment with either chondroitin sulfate (*CS1*), non-sulfated hyaluronic acid (*HA*), or sHA1 or without treatment by zymography (*A*). Analogously, the abundance of tissue inhibitor of metalloproteinases (TIMP)-3, a marker for reduced ECM remodeling, as determined by ELISA (*B*). ***, p value < 0.001; **, p value < 0.01, $n = 6$. All assays prepared with conditioned cell media.

various cell surface and ECM components (58). The up-regulated periostin (POSTN, FC = 1.9) is also involved in fibrillogenesis by supporting the cross-linking of ECM structural components (59).

Furthermore, with the cysteine-rich protein 61 (CCN1), a growth factor corresponding to the CCN protein family (60) was identified in higher abundance (FC = 3.4) after sHA1 treatment. CCN1 binds to various integrins and heparan sulfate proteoglycans and additionally supports the cell adhesion, *e.g.* of fibroblasts (61). Moreover, in comparative analysis to CS1, the growth factor CCN2 was identified to be up-regulated by sHA1 (FC = 2.6). Both CCN family members were shown to induce the osteoblastogenesis (62–64).

Altered MV Proteome Affects Matrix Remodeling—MMPs are a family of structurally related metalloendopeptidases (metalloproteinases), which are responsible for the homeostasis and turnover of the ECM. MMP activity is tightly regulated at the level of gene transcription, by proteolytic activation of the inactive proenzymes and by inhibition of the active enzyme by TIMPs (65).

The crucial roles for bone remodeling MMPs and their corresponding inhibitors were investigated in more detail. As shown above (Fig. 6*A*), many proteins regulated by sHA1 were identified in the functional cluster of proteinases and inhibitors. In the proteomics analysis, the ECM-degrading MMP-2 (gelatinase A) and TIMP2 and -3 were found to be up-regulated (FCs 2.8, 2.0, and 3.1).

To investigate changes in the matrix remodeling independently, MMP activity in conditioned cell culture medium was analyzed by zymography. The results of the densitometric evaluation showed a significant reduction of gelatinolytic activity by any tested GAG derivative ranging from 52 to 85% compared with untreated cells (Fig. 7*A*). The differences between the results from our proteomics analysis and the additional zymography can be attributed to the fact that the MMP2 protein load does not reflect the overall enzyme activity of

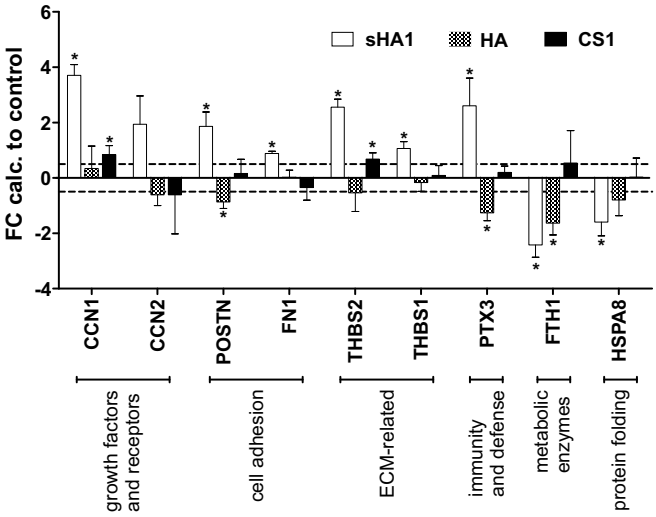

FIG. 8. **Comparison of GAG effects on protein abundance of individual proteins.** For selected matrix vesicle proteins that were found to be significantly regulated in response to at least one GAG, the quantitative values are presented as fold changes compared with control. *Asterisks* indicate values being significantly regulated proteins compared with control. *, p value < 0.05, $n = 3$.

MMP2. This supports the finding that the concentration of several putative inhibitors of MMP2, namely TIMP2 and TIMP3 and also THBS1 and THBS2, were significantly up-regulated with sHA1. This finding was independently proven by a TIMP3 ELISA (Fig. 7*B*), which showed that sHA1 induced a significant increase of TIMP3 protein level in comparison with the control (4.4-fold, p value < 0.001), whereas CS1 and HA did not.

Modulation of the MV Proteome by Other GAGs—To investigate whether HA and CS1 cause similar effects and whether the effects were modulated by sulfation (sHA1 *versus* HA), a different position of the sulfate group and/or different disaccharide units (sHA1 *versus* CS1), the MV proteome of sHA1-treated cells was compared with those of hBMSC treated with HA or CS1 (Fig. 8 and supplemental Table 2*G*). For a clearer illustration, all values were recalculated to control as references. All proteins that were quantified reliably in all comparisons and found to be regulated in at least one of the comparisons were considered. Using the Student's t test (two-tailed, unpaired), significantly regulated proteins compared with the control (FC $> \pm 0.5$, p value<0.05) were checked. Although a tendency toward altered abundance of the analyzed proteins in the presence of HA or CS1 was observed, a significant regulation could not be detected by the t test for the majority of the proteins. In most cases, significantly altered protein abundances were only observed after sHA1 treatment. However, the following five proteins were identified as being significantly regulated in the presence of HA or CS1: (i) CCN1 and THBS2 were up-regulated in the presence of CS1 (FC $= 0.8$ and 0.6 compared with the untreated control). As discussed earlier, both proteins are involved in cell adhesion and, moreover, osteoblast differentiation either directly by increasing the BMP synthesis (62) or indirectly by the activation of TGF-β (54). (ii) POSTN, the Pentraxin-related protein 3 (PTX3), and the FTH1 were significantly down-regulated in the presence of HA (FC $= -0.9$, -1.3, and -1.6 compared with the untreated control). Furthermore, (iii) proteins that were exclusively regulated in comparison with CS1 were identified, including three proteins that are crucial for ECM binding and the bone-forming process (supplemental Table 2*H*). CD44 and integrin β3 (ITGB3) were up-regulated by CS1 compared with sHA1 (FC $= 1.0$ and 3.2). Both proteins are known to play an important role in cell-to-cell and cell-to-matrix interactions. CD44 shows affinity to FN1 (66), whereas ITGB3 was shown to bind to the structural ECM protein osteopontin (67). Furthermore, in the presence of CS1, a tubulin component (TUBA4A) was also found to be up-regulated compared with sHA1. A disturbed assembly of microtubule was shown to enhance BMP2 and bone formation (68). No exclusive regulations after HA treatment could be observed.

Comparison of the Matrix Vesicle Proteome with hBMSC Proteome

Quantified and Regulated Proteins in hBMSC—In addition to examining the effects of different GAG derivatives on the MV proteome, their influence on the cell proteome was also analyzed (supplemental Table 3, *A* and *B*). A total of 1,559 proteins with 12,197 corresponding peptides were identified. In the comparison of the proportions of regulated proteins in MVs and in cell samples, it became obvious that GAG derivatives did not affect the cellular proteome as much as the MV proteome (Fig. 5). Compared with the control, 14 of a total of 487 reliably quantified proteins were up-regulated after sHA1 treatment (3%), whereas 9 were down-regulated (2%). Similar effects were found compared with HA (16 of 453 up and 5 down). Slightly more proteins were identified as regulated with sHA1 compared with CS1 (16 of 548 up and 15 down). This is consistent with the observations for the MV proteome.

Differences and Similarities between MV and hBMSC—Similar to the MV proteins, all reliably quantified proteins detected in the cellular fraction after sHA1 treatment were functionally clustered. To indicate differences to the MV fraction, the same categories were used (Fig. 6*B*). Interestingly, the majority of the proteins does not correspond to the functional clusters affecting the ECM organization and growth factor bioavailability as been found in the MVs. Opposite the MV proteome, the major functional clusters of quantified and regulated proteins correspond to metabolic enzymes and cytoskeletal proteins. Interestingly, more than 50 quantified proteins correspond to vesicle-attributed processes highlighting again their outstanding role in osteoblasts. However, none of those proteins were significantly regulated on the cellular level after sHA1 treatment. Similar to the MV fraction, three pro-

teins of the cluster of proteases and inhibitors were regulated in the cells representing a rather high proportion of all regulated proteins, also including the up-regulated MMP2 (FC = 2.6). In the proportionally low represented cluster of ECM-related proteins, two proteins were significantly regulated, namely THBS2 (FC = 3.0) and the collagen, type V, α-1 chain (COL5A1, FC = 2.0). The functional cluster of growth factors and receptors is represented by only eight proteins but contains two up-regulated proteins, namely CCN2 (FC = 2.8) and the insulin-like growth factor-binding protein 7 (IGFBP7, FC = 3.1), and one down-regulated protein, namely the fibroblast growth factor 2 (FGF2, FC = −1.6) protein. The overlap of co-regulated proteins in the MV fraction and the cellular fraction after sHA1 treatment compared to the control is very small and consists of only three proteins (MMP2, THBS2 and CCN2). This is also consistent with the comparisons of sHA1 to HA or CS1 (supplemental Table 3, *C* and *D*). However, by including quantitative values of non-regulated but reliably quantified proteins (n = 3, mean <S.D.) all proteins show the same tendencies in abundance.

DISCUSSION

An estimated 5–10% of bone fractures fail to heal properly, a percentage that might increase even further in the future due to alteration of the age pyramid and lifestyle of the population and related co-morbidities (*e.g.* diabetes mellitus or vascular diseases) and medication (*e.g.* with corticosteroids or statins) making bone implants one of the most in-demand biomaterials (69, 70). Some strategies to accelerate wound healing have already been adopted, and several osteoinductive biomaterials are currently used in therapy (71). One strategy is to design composite materials coated with artificial ECM (aECM) using proteins and sulfated GAGs (3).

Ideally, an implant coating should support bone formation and reduce resorption combined with a proper control of the immune reaction. Indeed, it has been shown that synthetically sulfated GAG derivatives promote osteogenic differentiation of human mesenchymal stromal cells and influence manifold cellular functions (14, 25, 27). Additionally, sulfated GAGs were shown to inhibit the bone degradation by osteoclasts (72) and to provide immunomodulation properties (73).

Especially to draw conclusions on the effect on bone formation *in vitro,* the cellular system should allow the study of all characteristic phases of the osteoblast life cycle. This includes an early differentiation phase characterized by expression and synthesis of ECM components, followed by ECM maturation and ending with mineralization of the ECM (74, 75). Therefore, primary hBMSC served as a cellular model and were differentiated into osteoblasts by the use of an osteogenic medium. MVs and the cellular proteome were collected over a period of 22 days.

Previous proteomic studies on GAG influence on osteoblasts revealed on the cellular level a strengthened cell-matrix interaction by integrins and vinculin as well as a decreased matrix remodeling after a treatment with sulfated GAGs, but the overall effect on the osteoblast proteome was rather small. Nevertheless, up-regulated proteins involved in the exo-/endocytosis system of the cells indicate effects on the matrix vesicle release and therefore activity of osteoblasts (25).

However, whether sulfated GAGs actually affect MV activity, whether the MV proteome or only the number of MV is altered, and, finally, which MV pathways and biological processes are regulated were not yet evaluated. Indeed, an increased mineral deposition combined with an increased TNAP activity in MV after a treatment with sulfated GAGs confirmed the first hypothesis. To investigate molecular effects in greater depth we applied MV proteomics.

As Wuthier and Lipscomb (1) reported in their recent review, the main challenge in MV proteomics, besides the limited availability of material, is to obtain sufficient MV purity. We slightly modified a protocol based on several centrifugation steps as recently published by Xiao *et al.* (24). As a quality control measure, we evaluated the presence of marker proteins, the presence of typical extracellular proteins, and the presence of proteins assigned to the major MV processes as well as the TNAP activity of the purified MV fraction. We concluded that the enrichment of MV proteins was successful because of the following: (i) 21 of the major 25 EV proteins were present in hBMSC-derived MV; (ii) the majority of 81% of identified proteins were either shown or predicted to be part of EVs; (iii) only a minority of 32% of the identified proteins included a signal peptide to be secreted by classical mechanisms; (iv) with 9% of the identified proteins the functional cluster of proteins being annotated to be involved in mineralization was strongly enriched; and (v) the released and collected MVs showed indispensable TNAP activity. Although artifact proteins cannot be completely excluded, proteins had to meet stringent criteria to be treated as quantified so that potential artifacts were assumed to be negligible.

As a first general finding of the proteome analysis, we observed that natural GAGs such as HA and CS1 and the low-sulfated HA derivative sHA1 had a greater impact on the proteome of MV (27–37% of proteins were found to be regulated) than on the cellular proteome (5–6% of the proteins were regulated). The functional clustering of regulated proteins from MVs and hBMSC revealed a larger enrichment of proteins crucial for bone formation in MVs (supplemental Tables 2, *F* and 3*E*). Taken together, this indicates that the observed promoting effect of sulfated hyaluronan on the ECM mineralization is to a large extent relying on an alteration in the MV composition. This seems not surprising, because MVs were shown to have a major role in the ECM mineralization driven by osteoblasts (23, 76). Despite its outstanding role, the number of studies dealing with MVs is rather low.

The collected MVs represent all characteristic phases of the osteoblast life cycle. Thus, a finding of activators and inhibitors or marker proteins of distinct differentiation states in

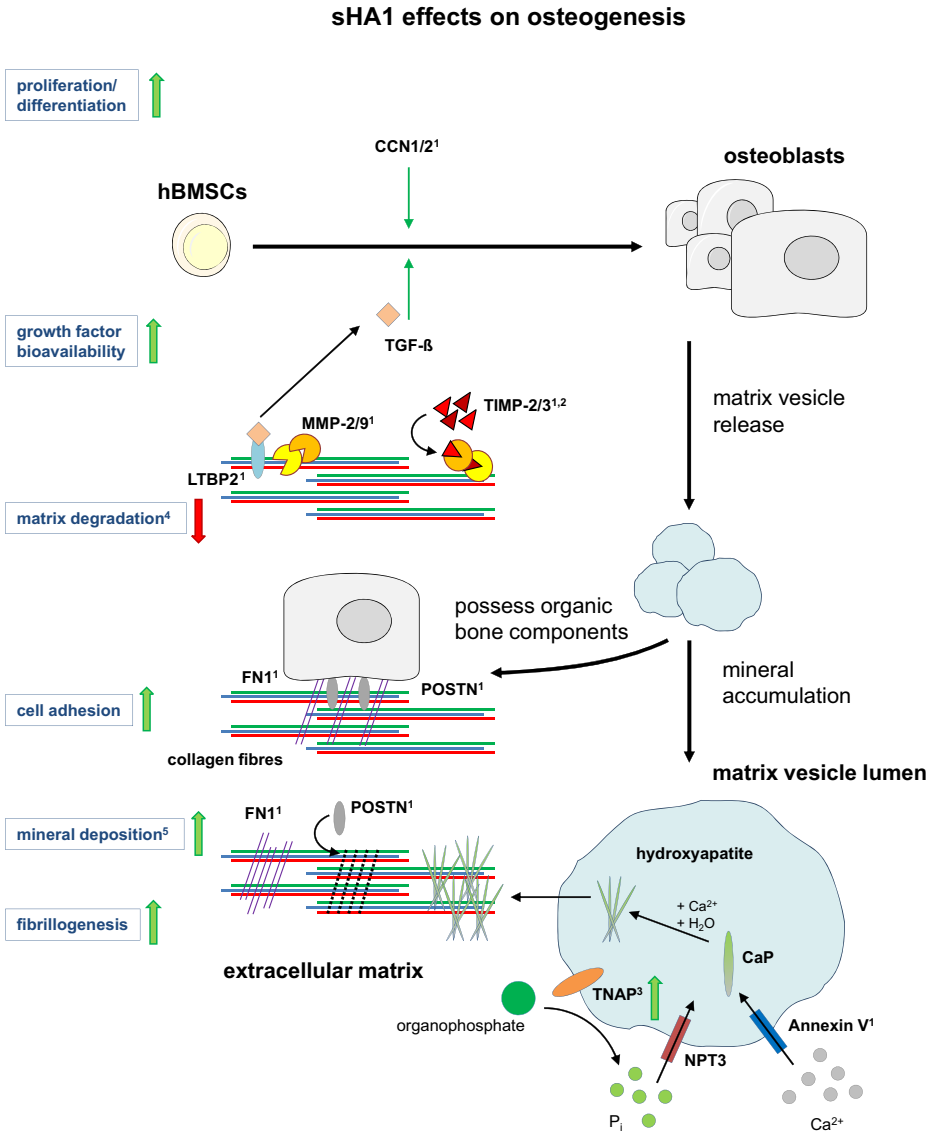

FIG. 9. **Summary of effects of sHA1 on osteogenesis.** Influence of *sHA1* on osteogenesis by an altered activity and composition of matrix vesicles. Evidence was gained by quantitative proteomics (*1*), ELISA (*2*), TNAP activity assay (*3*), zymography (*4*), or calcium and phosphate determination (*5*).

different modes of regulation or activation is not surprising. For example, MMP2 was identified to be up-regulated in terms of abundance after an sHA1 treatment, but the catalytic activity was decreased. This gelatinolytic active enzyme was shown to be expressed by osteoblasts previously (77, 78), and its catalytic activity has a major impact on a proper bone formation in humans *in vivo*. It could be assumed that MMP2 is required for MVs to reach deeper ECM layers to initiate mineralization and to release growth factors bound to the ECM in the early stages of development, although the overall activity of ECM-degrading proteins needs to be declined for proper ECM maturing and further bone formation. This is provided by an sHA1-induced pronounced increase of different MMP inhibitors to decrease the overall ECM degradation. Among those, TIMP3, which is the only one among four TIMPs that is tightly anchored in the pericellular matrix, interacts with sulfated GAG as shown for heparin and chondroitin sulfate (79, 80). As shown before, after sHA1 exposition most prominent regulated proteins were found in biological function of cell-matrix interaction, ECM organization, and regulation of growth factor bioavailability (Fig. 9). An increased interaction between MVs and the cell, respectively, with ECM components by released linker proteins like thrombospondins and FN1 appears convincing. FN1 positively stimulates osteoblast differentiation and survival (81, 82) and seems to be the nuclei for mineralization cores in the ECM (83). This mineralization seems to be additionally supported by THBS2 (84). The ECM fibrillogenesis may be provided by a higher abundance of POSTN after sHA1 stimulation. It recruits the BMP1 to FN1, which leads to the activation of lysyl oxidase, an enzyme that is responsible for cross-linking of tropocollagen in the ECM (59). Additionally the bioavailability of TGF-β, the most prominent inducer of ECM protein expression, is potentially affected by the up-regulated LTBP2. By this, a higher amount of

TGF-β could be stored in the ECM and released by ECM degradation (57). Through up-regulated THBS1 and -2, TGF-β is activated (54), which in turn positively stimulates the osteoblast maturing from hBMSC (85). However, the up-regulated FBN1 was shown to impair a proper TGF-β formation but increases the bioavailability of the BMP2, another stimulus of osteoblastogenesis (56, 86). With CCN1 and CCN2, two growth factors were identified as up-regulated directly after sHA1 exposition. Both proteins are expressed Wnt-dependent in the osteoblastogenesis. CCN1 was shown to induce the osteoblastogenesis by an increased BMP2 expression and represses the osteoclastic phenotype by an integrin-independent mechanism, whereas CCN2 was shown to induce osteogenesis *in vitro* and *in vivo* (62–64, 87, 88). Furthermore, with FTH1, a potential inhibitor of osteogenesis, a protein also corresponding to the cluster of metabolic enzymes was down-regulated in our findings. The repressing effect on the development of the osteoblastic phenotype could be attributed to its ferroxidase activity (89). In sum, this lead to a more efficient maturing of hBMSC to osteoblasts, a stronger interaction of cells and released MVs with the ECM, and a stronger ECM mineralization as observed *in vitro* after sHA1 exposition.

As observed, desmoglein-1 was down-regulated in MVs by sHA1. Desmoglein-1 is a cadherin family glycoprotein occurring in all desmosomes and is involved in calcium-dependent cell-to-cell interactions via intermediate filaments (90). This could lead to decreased cell-to-cell interaction. With the PTX3, we identified another protein that was down-regulated after sHA1 exposition with yet unknown function in osteoblasts. PTX3 was identified in the secretome of adipose-derived stem cells (Asks), a novel source for therapeutics that was indeed shown to comprise several stimulators for osteoblasts and osteoclasts (91).

A fine-tuning of the cellular response of osteoblasts on different GAGs seems possible, because the presence or absence of sHA1, HA, or CS1 affects the abundance of some specific proteins as already shown. For example, CS1 increased the abundance of CD44 and ITGB3, both of which are known to participate in cell adhesion to the ECM (66, 67). Because CD44 binding to FN1 is dependent on a modification of CD44 with chondroitin sulfate, and the presence of soluble CS1 was shown to inhibit this binding, this up-regulation could suggest the existence of a feedback loop. CCN1 and THBS2, two proteins with a positive influence on osteogenesis, were also up-regulated after CS1 exposition but not to the same extent as after sHA1 exposition. Although the presence of HA decreases the abundance of FTH1, which was shown to inhibit osteogenesis (89), proper ECM organization could be impaired under those conditions as a result of POSTN abundance also being decreased.

Of the 51 proteins quantified in the MV fraction, 27 were also quantified in the hBMSC proteome analysis after sHA1 treatment compared with the control. This moderate overlap might be explained by a combination of sampling (cellular proteomes have a much higher complexity than MV proteomes) or sensitivity (proteins are enriched in the MV fraction) issues. Only three proteins were found to be regulated in cells and MVs, although the majority of the 16 proteins are exclusively regulated in MVs and not in cells after sHA1 treatment. This indicates that the MV proteome composition is somehow directly regulated by GAGs.

Although previous studies have focused on the binding of sulfated GAGs to proteins, and several binding partners are already known (5), the mechanisms of cellular response to GAG-protein complexes are still only poorly understood, and further studies in this area are needed.

Taken together, besides slight changes in the protein composition of MVs after CS1 or HA exposition, sHA1 induced mainly positive effects on the osteoblastic phenotype in terms of mineralization, TNAP activity, and ECM degradation as well as on protein abundance. The use of mixed solutions could be discussed in the future as a means of fine-tuning cellular responses to GAGs.

The use of sulfated GAGs could be a promising approach in bone grafting because *in vitro* studies showed promoting effects on osteogenesis (3, 14). However, besides stimulating bone formation and reducing bone resorption, the alteration of GAG concentrations has also been reported to correlate with cancer progression by activating oncogenic pathways (92), promoting invasion and metastasis (93), and accelerating shedding of extracellular vesicles (94, 95), which have to be carefully evaluated prior to clinical application. An alternative approach could be provided by dexamethasone, a synthetic glucocorticoid that was also shown to stimulate an osteoblast phenotype *in vivo* (96). Future studies need to investigate a potentially accumulated influence of GAGs and dexamethasone on bone formation.

Concluding Remarks—In conclusion, sulfated hyaluronan significantly affects the composition and enhances the activity of matrix vesicles of osteoblasts and thus also matrix formation, mineralization, and remodeling. In this study, the observed changes in relative protein abundances caused by GAGs were stronger than those observed for the intracellular proteins, highlighting the importance of matrix vesicle regulation as a regulated process for the modulation of osteoblast activity. Moreover, the study provided an opportunity to sensitively measure effects of implant coating compounds such as sulfated GAGs.

Interestingly, the different GAGs resulted not only in different amplitudes but also in different functional effects. This might open up a new route to modulate MV activity and thus finally improve bone formation and treat bone defects *in vivo*.

Acknowledgment—We thank Jacqueline Kobelt for technical assistance.

* This work was supported by Deutsche Forschungsgemeinschaft Transregio 67 Subprojects A2, B1, and Z4. The authors declare that they have no conflicts of interest with the contents of this article.

S This article contains supplemental Tables S1 to S3.

§ Both authors contributed equally to this work.

¶ Present address: B CUBE Center for Molecular Bioengineering, University of Technology, Dresden, 01307 Dresden, Germany.

|||| To whom correspondence may be addressed: Dept. of Proteomics, UFZ, Helmholtz Centre for Environmental Research, Permoserstrasse 15, 04318 Leipzig, Germany. Tel.: 49-341-2351354; Fax: 49-341-2351786; E-mail: Stefan.Kalkhof@ufz.de; and Institute of Physiological Chemistry, Medical Theoretical Center, University of Technology, Dresden, Fiedlerstrasse 42, 01307 Dresden, Germany. Tel.: 49-351-458-6430; Fax: +49-351-4586305; E-mail: Ute.Hempel@tu-dresden.de.

REFERENCES

1. Wuthier, R. E., and Lipscomb, G. F. (2011) Matrix vesicles: structure, composition, formation and function in calcification. *Front. Biosci.* **16,** 2812–2902
2. Ling, L., Murali, S., Stein, G. S., van Wijnen, A. J., and Cool, S. M. (2010) Glycosaminoglycans modulate RANKL-induced osteoclastogenesis. *J. Cell. Biochem.* **109,** 1222–1231
3. Salbach, J., Rachner, T. D., Rauner, M., Hempel, U., Anderegg, U., Franz, S., Simon, J. C., and Hofbauer, L. C. (2012) Regenerative potential of glycosaminoglycans for skin and bone. *J. Mol. Med.* **90,** 625–635
4. Esko, J. D., Kimata, K., and Lindahl, U. (2009) in *Essentials of Glycobiology* (Varki, A., Cummings, R. D., Esko, J. D., Freeze, H. H., Stanley, P., Bertozzi, C. R., Hart, G. W., and Etzler, M. E., eds) 2nd Ed., Cold Spring Harbor Laboratory Press, Cold Spring Harbor. NY, 229–248
5. Gandhi, N. S., and Mancera, R. L. (2008) The structure of glycosaminoglycans and their interactions with proteins. *Chem. Biol. Drug Des.* **72,** 455–482
6. Hintze, V., Moeller, S., Schnabelrauch, M., Bierbaum, S., Viola, M., Worch, H., and Scharnweber, D. (2009) Modifications of hyaluronan influence the interaction with human bone morphogenetic protein-4 (hBMP-4). *Biomacromolecules* **10,** 3290–3297
7. Kunze, R., Rösler, M., Möller, S., Schnabelrauch, M., Riemer, T., Hempel, U., and Dieter, P. (2010) Sulfated hyaluronan derivatives reduce the proliferation rate of primary rat calvarial osteoblasts. *Glycoconj. J.* **27,** 151–158
8. Lamoureux, F., Baud'huin, M., Duplomb, L., Heymann, D., and Rédini, F. (2007) Proteoglycans: key partners in bone cell biology. *Bioessays* **29,** 758–771
9. Pieper, J. S., van Wachem, P. B., van Luyn, M. J. A., Brouwer, L. A., Hafmans, T., Veerkamp, J. H., and van Kuppevelt, T. H. (2000) Attachment of glycosaminoglycans to collagenous matrices modulates the tissue response in rats. *Biomaterials* **21,** 1689–1699
10. Prestwich, G. D. (2008) Engineering a clinically useful matrix for cell therapy. *Organogenesis* **4,** 42–47
11. Roughley, P. J. (2006) The structure and function of cartilage proteoglycans. *Eur. Cell Mater.* **12,** 92–101
12. Sasisekharan, R., Raman, R., and Prabhakar, V. (2006) Glycomics approach to structure-function relationships of glycosaminoglycans. *Annu. Rev. Biomed. Eng.* **8,** 181–231
13. Souza-Fernandes, A. B., Pelosi, P., and Rocco, P. R. (2006) Bench-to-bedside review: the role of glycosaminoglycans in respiratory disease. *Crit. Care* **10,** 237
14. Hempel, U., Preissler, C., Vogel, S., Möller, S., Hintze, V., Becher, J., Schnabelrauch, M., Rauner, M., Hofbauer, L. C., and Dieter, P. (2014) Artificial extracellular matrices with oversulfated glycosaminoglycan derivatives promote the differentiation of osteoblast-precursor cells and premature osteoblasts. *Biomed. Res. Int.* **2014,** 938368
15. Dombrowski, C., Song, S. J., Chuan, P., Lim, X., Susanto, E., Sawyer, A. A., Woodruff, M. A., Hutmacher, D. W., Nurcombe, V., and Cool, S. M. (2009) Heparan sulfate mediates the proliferation and differentiation of rat mesenchymal stem cells. *Stem Cells Dev.* **18,** 661–670
16. Hoshiba, T., Kawazoe, N., Tateishi, T., and Chen, G. (2009) Development of stepwise osteogenesis-mimicking matrices for the regulation of mesenchymal stem cell functions. *J. Biol. Chem.* **284,** 31164–31173
17. Anderson, H. C. (2003) Matrix vesicles and calcification. *Curr. Rheumatol. Rep.* **5,** 222–226
18. Hale, J. E., and Wuthier, R. E. (1987) The mechanism of matrix vesicle formation. Studies on the composition of chondrocyte microvilli and on the effects of microfilament-perturbing agents on cellular vesiculation. *J. Biol. Chem.* **262,** 1916–1925
19. Thouverey, C., Strzelecka-Kiliszek, A., Balcerzak, M., Buchet, R., and Pikula, S. (2009) Matrix vesicles originate from apical membrane microvilli of mineralizing osteoblast-like Saos-2 cells. *J. Cell. Biochem.* **106,** 127–138
20. Choi, D. S., Kim, D. K., Kim, Y. K., and Gho, Y. S. (2015) Proteomics of extracellular vesicles: exosomes and ectosomes. *Mass Spectrom. Rev.* **34,** 474–490
21. Wuthier, R. E. (1975) Effect of phospholipids on the transformation of amorphous calcium phosphate to hydroxapatite *in vitro*. *Calcif. Tissue Res.* **19,** 197–210
22. Anderson, H. C. (1995) Molecular biology of matrix vesicles. *Clin. Orthop. Relat. Res*. **314,** 266–280
23. Golub, E. E. (2009) Role of matrix vesicles in biomineralization. *Biochim. Biophys. Acta* **1790,** 1592–1598
24. Xiao, Z., Camalier, C. E., Nagashima, K., Chan, K. C., Lucas, D. A., de la Cruz, M. J., Gignac, M., Lockett, S., Issaq, H. J., Veenstra, T. D., Conrads, T. P., and Beck, G. R., Jr. (2007) Analysis of the extracellular matrix vesicle proteome in mineralizing osteoblasts. *J. Cell. Physiol.* **210,** 325–335
25. Kliemt, S., Lange, C., Otto, W., Hintze, V., Möller, S., von Bergen, M., Hempel, U., and Kalkhof, S. (2013) Sulfated hyaluronan containing collagen matrices enhance cell-matrix interaction, endocytosis, and osteogenic differentiation of human mesenchymal stromal cells. *J. Proteome Res.* **12,** 378–389
26. Oswald, J., Boxberger, S., Jørgensen, B., Feldmann, S., Ehninger, G., Bornhäuser, M., and Werner, C. (2004) Mesenchymal stem cells can be differentiated into endothelial cells *in vitro*. *Stem Cells* **22,** 377–384
27. Hempel, U., Hefti, T., Kalbacova, M., Wolf-Brandstetter, C., Dieter, P., and Schlottig, F. (2010) Response of osteoblast-like SAOS-2 cells to zirconia ceramics with different surface topographies. *Clin. Oral Implants Res.* **21,** 174–181
28. Lutter, A. H., Hempel, U., Wolf-Brandstetter, C., Garbe, A. I., Goettsch, C., Hofbauer, L. C., Jessberger, R., and Dieter, P. (2010) A novel resorption assay for osteoclast functionality based on an osteoblast-derived native extracellular matrix. *J. Cell. Biochem.* **109,** 1025–1032
29. Schwab, W., Galbiati, F., Volonte, D., Hempel, U., Wenzel, K. W., Funk, R. H., Lisanti, M. P., and Kasper, M. (1999) Characterisation of caveolins from cartilage: expression of caveolin-1, -2 and -3 in chondrocytes and in alginate cell culture of the rat tibia. *Histochem. Cell Biol.* **112,** 41–49
30. Müller, S. A., Kohajda, T., Findeiss, S., Stadler, P. F., Washietl, S., Kellis, M., von Bergen, M., and Kalkhof, S. (2010) Optimization of parameters for coverage of low molecular weight proteins. *Anal. Bioanal. Chem.* **398,** 2867–2881
31. Cox, J., and Mann, M. (2008) MaxQuant enables high peptide identification rates, individualized p.p.b.-range mass accuracies and proteome-wide protein quantification. *Nat. Biotechnol.* **26,** 1367–1372
32. Cox, J., Neuhauser, N., Michalski, A., Scheltema, R. A., Olsen, J. V., and Mann, M. (2011) Andromeda: a peptide search engine integrated into the MaxQuant environment. *J. Proteome Res.* **10,** 1794–1805
33. Vizcaíno, J. A., Deutsch, E. W., Wang, R., Csordas, A., Reisinger, F., Ríos, D., Dianes, J. A., Sun, Z., Farrah, T., Bandeira, N., Binz, P. A., Xenarios, I., Eisenacher, M., Mayer, G., Gatto, L., Campos, A., Chalkley, R. J., Kraus, H. J., Albar, J. P., Martinez-Bartolomé, S., Apweiler, R., Omenn, G. S., Martens, L., Jones, A. R., and Hermjakob, H. (2014) ProteomeXchange provides globally coordinated proteomics data submission and dissemination. *Nat. Biotechnol.* **32,** 223–226
34. Baker, P. R., and Chalkley, R. J. (2014) MS-viewer: a web-based spectral viewer for proteomics results. *Mol. Cell. Proteomics* **13,** 1392–1396
35. Mi, H., Muruganujan, A., Casagrande, J. T., and Thomas, P. D. (2013) Large-scale gene function analysis with the PANTHER classification system. *Nat. Protoc.* **8,** 1551–1566
36. Petersen, T. N., Brunak, S., von Heijne, G., and Nielsen, H. (2011) SignalP 4.0: discriminating signal peptides from transmembrane regions. *Nat. Methods* **8,** 785–786
37. Mathivanan, S., Fahner, C. J., Reid, G. E., and Simpson, R. J. (2012) ExoCarta 2012: database of exosomal proteins, RNA and lipids. *Nucleic Acids Res.* **40,** D1241–D1244
38. Mathivanan, S., Lim, J. W., Tauro, B. J., Ji, H., Moritz, R. L., and Simpson,

R. J. (2010) Proteomics analysis of A33 immunoaffinity-purified exosomes released from the human colon tumor cell line LIM1215 reveals a tissue-specific protein signature. *Mol. Cell. Proteomics* **9,** 197–208
39. Simpson, R., Kalra, H., and Mathivanan, S. (2012) ExoCarta as a resource for exosomal research. *J. Extracell. Vesicles* **1,** 18374
40. Bandorowicz-Pikula, J., and Pikula, S. (1998) Modulation of annexin VI–driven aggregation of phosphatidylserine liposomes by ATP. *Biochimie* **80,** 613–620
41. Sapir-Koren, R., and Livshits, G. (2011) Bone mineralization and regulation of phosphate homeostasis. *IBMS BoneKEy* **8,** 286–300
42. Yoshioka, Y., Konishi, Y., Kosaka, N., Katsuda, T., Kato, T., and Ochiya, T. (2013) Comparative marker analysis of extracellular vesicles in different human cancer types. *J. Extracell. Vesicles* **2,** 20424
43. Mathivanan, S., and Simpson, R. J. (2009) ExoCarta: a compendium of exosomal proteins and RNA. *Proteomics* **9,** 4997–5000
44. Bard, M. P., Hegmans, J. P., Hemmes, A., Luider, T. M., Willemsen, R., Severijnen, L. A., van Meerbeeck, J. P., Burgers, S. A., Hoogsteden, H. C., and Lambrecht, B. N. (2004) Proteomic analysis of exosomes isolated from human malignant pleural effusions. *Am. J. Respir. Cell Mol. Biol.* **31,** 114–121
45. Mears, R., Craven, R. A., Hanrahan, S., Totty, N., Upton, C., Young, S. L., Patel, P., Selby, P. J., and Banks, R. E. (2004) Proteomic analysis of melanoma-derived exosomes by two-dimensional polyacrylamide gel electrophoresis and mass spectrometry. *Proteomics* **4,** 4019–4031
46. Street, J. M., Barran, P. E., Mackay, C. L., Weidt, S., Balmforth, C., Walsh, T. S., Chalmers, R. T., Webb, D. J., and Dear, J. W. (2012) Identification and proteomic profiling of exosomes in human cerebrospinal fluid. *J. Transl. Med.* **10,** 5
47. Welton, J. L., Khanna, S., Giles, P. J., Brennan, P., Brewis, I. A., Staffurth, J., Mason, M. D., and Clayton, A. (2010) Proteomics analysis of bladder cancer exosomes. *Mol. Cell. Proteomics* **9,** 1324–1338
48. Sandvig, K., and Llorente, A. (2012) Proteomic analysis of microvesicles released by the human prostate cancer cell line PC-3. *Mol. Cell. Proteomics* **11,** M111.012914
49. Schimmöller, F., Simon, I., and Pfeffer, S. R. (1998) Rab GTPases, directors of vesicle docking. *J. Biol. Chem.* **273,** 22161–22164
50. Daley, W. P., Peters, S. B., and Larsen, M. (2008) Extracellular matrix dynamics in development and regenerative medicine. *J. Cell Sci.* **121,** 255–264
51. D'Angelo, M., Billings, P. C., Pacifici, M., Leboy, P. S., and Kirsch, T. (2001) Authentic matrix vesicles contain active metalloproteases (MMP). A role for matrix vesicle-associated MMP-13 in activation of transforming growth factor-β. *J. Biol. Chem.* **276,** 11347–11353
52. Raynal, P., and Pollard, H. B. (1994) Annexins: the problem of assessing the biological role for a gene family of multifunctional calcium- and phospholipid-binding proteins. *Biochim Biophys. Acta* **1197,** 63–93
53. Tan, K., Duquette, M., Liu, J. H., Zhang, R., Joachimiak, A., Wang, J. H., and Lawler, J. (2006) The structures of the thrombospondin-1 N-terminal domain and its complex with a synthetic pentameric heparin. *Structure* **14,** 33–42
54. Lawler, J. (2000) The functions of thrombospondin-1 and-2. *Curr. Opin. Cell Biol.* **12,** 634–640
55. Bein, K., and Simons, M. (2000) Thrombospondin type 1 repeats interact with matrix metalloproteinase 2. Regulation of metalloproteinase activity. *J. Biol. Chem.* **275,** 32167–32173
56. Nistala, H., Lee-Arteaga, S., Smaldone, S., Siciliano, G., Carta, L., Ono, R. N., Sengle, G., Arteaga-Solis, E., Levasseur, R., Ducy, P., Sakai, L. Y., Karsenty, G., and Ramirez, F. (2010) Fibrillin-1 and -2 differentially modulate endogenous TGF-β and BMP bioavailability during bone formation. *J. Cell Biol.* **190,** 1107–1121
57. Dallas, S. L., Miyazono, K., Skerry, T. M., Mundy, G. R., and Bonewald, L. F. (1995) Dual role for the latent transforming growth factor-β binding protein in storage of latent TGF-β in the extracellular matrix and as a structural matrix protein. *J. Cell Biol.* **131,** 539–549
58. Mao, Y., and Schwarzbauer, J. E. (2005) Fibronectin fibrillogenesis, a cell-mediated matrix assembly process. *Matrix Biol.* **24,** 389–399
59. Kudo, A. (2011) Periostin in fibrillogenesis for tissue regeneration: periostin actions inside and outside the cell. *Cell. Mol. Life Sci.* **68,** 3201–3207
60. Brigstock, D. R. (2003) The CCN family: a new stimulus package. *J. Endocrinol.* **178,** 169–175
61. Chen, N., Chen, C. C., and Lau, L. F. (2000) Adhesion of human skin fibroblasts to Cyr61 is mediated through integrin $\alpha 6\beta 1$ and cell surface heparan sulfate proteoglycans. *J. Biol. Chem.* **275,** 24953–24961
62. Su, J. L., Chiou, J., Tang, C. H., Zhao, M., Tsai, C. H., Chen, P. S., Chang, Y. W., Chien, M. H., Peng, C. Y., Hsiao, M., Kuo, M. L., and Yen, M. L. (2010) CYR61 regulates BMP-2-dependent osteoblast differentiation through the $\alpha v\beta 3$ integrin/integrin-linked kinase/ERK pathway. *J. Biol. Chem.* **285,** 31325–31336
63. Luo, Q., Kang, Q., Si, W., Jiang, W., Park, J. K., Peng, Y., Li, X., Luu, H. H., Luo, J., Montag, A. G., Haydon, R. C., and He, T. C. (2004) Connective tissue growth factor (CTGF) is regulated by Wnt and bone morphogenetic proteins signaling in osteoblast differentiation of mesenchymal stem cells. *J. Biol. Chem.* **279,** 55958–55968
64. Safadi, F. F., Xu, J., Smock, S. L., Kanaan, R. A., Selim, A. H., Odgren, P. R., Marks, S. C., Jr., Owen, T. A., and Popoff, S. N. (2003) Expression of connective tissue growth factor in bone: its role in osteoblast proliferation and differentiation *in vitro* and bone formation *in vivo*. *J. Cell. Physiol.* **196,** 51–62
65. Lowrey, G. E., Henderson, N., Blakey, J. D., Corne, J. M., and Johnson, S. R. (2008) MMP-9 protein level does not reflect overall MMP activity in the airways of patients with COPD. *Respir. Med.* **102,** 845–851
66. Jalkanen, S., and Jalkanen, M. (1992) Lymphocyte CD44 binds the COOH-terminal heparin-binding domain of fibronectin. *J. Cell Biol.* **116,** 817–825
67. Ross, F. P., Chappel, J., Alvarez, J. I., Sander, D., Butler, W. T., Farach-Carson, M. C., Mintz, K. A., Robey, P. G., Teitelbaum, S. L., and Cheresh, D. A. (1993) Interactions between the bone matrix proteins osteopontin and bone sialoprotein and the osteoclast integrin $\alpha v\beta 3$ potentiate bone resorption. *J. Biol. Chem.* **268,** 9901–9907
68. Zhao, M., Ko, S. Y., Liu, J. H., Chen, D., Zhang, J., Wang, B., Harris, S. E., Oyajobi, B. O., and Mundy, G. R. (2009) Inhibition of microtubule assembly in osteoblasts stimulates bone morphogenetic protein 2 expression and bone formation through transcription factor Gli2. *Mol. Cell. Biol.* **29,** 1291–1305
69. Mathieu, L. M., Mueller, T. L., Bourban, P. E., Pioletti, D. P., Müller, R., and Månson, J. A. (2006) Architecture and properties of anisotropic polymer composite scaffolds for bone tissue engineering. *Biomaterials* **27,** 905–916
70. Gaston, M. S., and Simpson, A. H. (2007) Inhibition of fracture healing. *J. Bone Joint Surg. Br.* **89,** 1553–1560
71. Barradas, A. M., Yuan, H., van Blitterswijk, C. A., and Habibovic, P. (2011) Osteoinductive biomaterials: current knowledge of properties, experimental models and biological mechanisms. *Eur. Cell Mater.* **21,** 407–429
72. Salbach, J., Kliemt, S., Rauner, M., Rachner, T. D., Goettsch, C., Kalkhof, S., von Bergen, M., Möller, S., Schnabelrauch, M., Hintze, V., Scharnweber, D., and Hofbauer, L. C. (2012) The effect of the degree of sulfation of glycosaminoglycans on osteoclast function and signaling pathways. *Biomaterials* **33,** 8418–8429
73. Franz, S., Allenstein, F., Kajahn, J., Forstreuter, I., Hintze, V., Möller, S., and Simon, J. C. (2013) Artificial extracellular matrices composed of collagen I and high-sulfated hyaluronan promote phenotypic and functional modulation of human pro-inflammatory M1 macrophages. *Acta Biomaterialia* **9,** 5621–5629
74. Becker, D., Geissler, U., Hempel, U., Bierbaum, S., Scharnweber, D., Worch, H., and Wenzel, K. W. (2002) Proliferation and differentiation of rat calvarial osteoblasts on type I collagen-coated titanium alloy. *J. Biomed. Mater. Res.* **59,** 516–527
75. Owen, T. A., Aronow, M., Shalhoub, V., Barone, L. M., Wilming, L., Tassinari, M. S., Kennedy, M. B., Pockwinse, S., Lian, J. B., and Stein, G. S. (1990) Progressive development of the rat osteoblast phenotype *in vitro*: reciprocal relationships in expression of genes associated with osteoblast proliferation and differentiation during formation of the bone extracellular matrix. *J. Cell. Physiol.* **143,** 420–430
76. Golub, E. E. (2011) Biomineralization and matrix vesicles in biology and pathology. *Semin. Immunopathol.* **33,** 409–417
77. Meikle, M. C., Bord, S., Hembry, R. M., Compston, J., Croucher, P. I., and Reynolds, J. J. (1992) Human osteoblasts in culture synthesize collagenase and other matrix metalloproteinases in response to osteotropic hormones and cytokines. *J. Cell Sci.* **103,** 1093–1099
78. Martignetti, J. A., Aqeel, A. A., Sewairi, W. A., Boumah, C. E., Kambouris, M., Mayouf, S. A., Sheth, K. V., Eid, W. A., Dowling, O., Harris, J., Glucksman, M. J., Bahabri, S., Meyer, B. F., and Desnick, R. J. (2001)

Mutation of the matrix metalloproteinase 2 gene (MMP2) causes a multicentric osteolysis and arthritis syndrome. *Nat. Genet.* **28,** 261–265
79. Yu, W. H., Yu, S., Meng, Q., Brew, K., and Woessner, J. F., Jr. (2000) TIMP-3 binds to sulfated glycosaminoglycans of the extracellular matrix. *J. Biol. Chem.* **275,** 31226–31232
80. Troeberg, L., Lazenbatt, C., Anower-E-Khuda, M. F., Freeman, C., Federov, O., Habuchi, H., Habuchi, O., Kimata, K., and Nagase, H. (2014) Sulfated glycosaminoglycans control the extracellular trafficking and the activity of the metalloprotease inhibitor TIMP-3. *Chem. Biol.* **21,** 1300–1309
81. Moursi, A. M., Globus, R. K., and Damsky, C. H. (1997) Interactions between integrin receptors and fibronectin are required for calvarial osteoblast differentiation *in vitro*. *J. Cell Sci.* **110,** 2187–2196
82. Globus, R. K., Doty, S. B., Lull, J. C., Holmuhamedov, E., Humphries, M. J., and Damsky, C. H. (1998) Fibronectin is a survival factor for differentiated osteoblasts. *J. Cell Sci.* **111,** 1385–1393
83. Daculsi, G., Pilet, P., Cottrel, M., and Guicheux, G. (1999) Role of fibronectin during biological apatite crystal nucleation: ultrastructural characterization. *J. Biomed. Mater. Res.* **47,** 228–233
84. Alford, A. I., Terkhorn, S. P., Reddy, A. B., and Hankenson, K. D. (2010) Thrombospondin-2 regulates matrix mineralization in MC3T3-E1 preosteoblasts. *Bone* **46,** 464–471
85. Noda, M., and Camilliere, J. J. (1989) *In vivo* stimulation of bone formation by transforming growth factor-β. *Endocrinology* **124,** 2991–2994
86. Yamaguchi, A., Katagiri, T., Ikeda, T., Wozney, J. M., Rosen, V., Wang, E. A., Kahn, A. J., Suda, T., and Yoshiki, S. (1991) Recombinant human bone morphogenetic protein-2 stimulates osteoblastic maturation and inhibits myogenic differentiation *in vitro*. *J. Cell Biol.* **113,** 681–687
87. Si, W., Kang, Q., Luu, H. H., Park, J. K., Luo, Q., Song, W. X., Jiang, W., Luo, X., Li, X., Yin, H., Montag, A. G., Haydon, R. C., and He, T. C. (2006) CCN1/Cyr61 is regulated by the canonical Wnt signal and plays an important role in Wnt3A-induced osteoblast differentiation of mesenchymal stem cells. *Mol. Cell Biol.* **26,** 2955–2964
88. Crockett, J. C., Schütze, N., Tosh, D., Jatzke, S., Duthie, A., Jakob, F., and Rogers, M. J. (2007) The matricellular protein CYR61 inhibits osteoclastogenesis by a mechanism independent of $\alpha v\beta 3$ and $\alpha v\beta 5$. *Endocrinology* **148,** 5761–5768
89. Zarjou, A., Jeney, V., Arosio, P., Poli, M., Zavaczki, E., Balla, G., and Balla, J. (2010) Ferritin ferroxidase activity: a potent inhibitor of osteogenesis. *J. Bone Miner. Res.* **25,** 164–172
90. Nilles, L. A., Parry, D. A., Powers, E. E., Angst, B. D., Wagner, R. M., and Green, K. J. (1991) Structural analysis and expression of human desmoglein: a cadherin-like component of the desmosome. *J. Cell Sci.* **99,** 809–821
91. Lee, K., Kim, H., Kim, J. M., Kim, J. R., Kim, K. J., Kim, Y. J., Park, S. I., Jeong, J. H., Moon, Y. M., Lim, H. S., Bae, D. W., Kwon, J., Ko, C. Y., Kim, H. S., Shin, H. I., and Jeong, D. (2011) Systemic transplantation of human adipose-derived stem cells stimulates bone repair by promoting osteoblast and osteoclast function. *J. Cell. Mol. Med.* **15,** 2082–2094
92. Bourguignon, L. Y., Shiina, M., and Li, J.-J. (2014) Hyaluronan–CD44 interaction promotes oncogenic signaling, microRNA functions, chemoresistance, and radiation resistance in cancer stem cells leading to tumor progression. *Adv. Cancer Res.* **123,** 255–275
93. Basappa, Rangappa, K. S., and Sugahara, K. (2014) Roles of glycosaminoglycans and glycanmimetics in tumor progression and metastasis. *Glycoconj. J.* **31,** 461–467
94. Rilla, K., Pasonen-Seppänen, S., Deen, A. J., Koistinen, V. V., Wojciechowski, S., Oikari, S., Kärnä, R., Bart, G., Törrönen, K., Tammi, R. H., and Tammi, M. I. (2013) Hyaluronan production enhances shedding of plasma membrane-derived microvesicles. *Exp. Cell Res.* **319,** 2006–2018
95. Rilla, K., Siiskonen, H., Tammi, M., and Tammi, R. (2014) Hyaluronan-coated extracellular vesicles: a novel link between hyaluronan and cancer. *Adv. Cancer Res.* **123,** 121–148
96. Song, I. H., Caplan, A. I., and Dennis, J. E. (2009) *In vitro* dexamethasone pretreatment enhances bone formation of human mesenchymal stem cells *in vivo*. *J. Orthop. Res.* **27,** 916–921